BIOCHEMISTRY
including biophysical chemistry & molecular biology

ARTICLE

pubs.acs.org/biochemistry

Understanding the Origins of Time-Dependent Inhibition by Polypeptide Deformylase Inhibitors

Rachel Totoritis, Chaya Duraiswami, Amy N. Taylor, John J. Kerrigan, Nino Campobasso, Katherine J. Smith, Paris Ward, Bryan W. King, Monique Murrayz-Thompson, Amber D. Jones, Glenn S. Van Aller, Kelly M. Aubart, Magdalena Zalacain, Sara H. Thrall, Thomas D. Meek, and Benjamin Schwartz*

Departments of Biological Reagents and Assay Development, Computational and Structural Sciences, and Antibacterials, GlaxoSmithKline, 1250 South Collegeville Road, Collegeville, Pennsylvania 19426, United States

Supporting Information

ABSTRACT: The continual bacterial adaptation to antibiotics creates an ongoing medical need for the development of novel therapeutics. Polypeptide deformylase (PDF) is a highly conserved bacterial enzyme, which is essential for viability. It has previously been shown that PDF inhibitors represent a promising new area for the development of antimicrobial agents, and that many of the best PDF inhibitors demonstrate slow, time-dependent binding. To improve our understanding of the mechanistic origin of this time-dependent inhibition, we examined in detail the kinetics of PDF catalysis and inhibition by several different PDF inhibitors. Varying pH and solvent isotope led to clear changes in time-dependent inhibition parameters, as did inclusion of NaCl, which binds to the active site metal of PDF. Quantitative analysis of these results demonstrated that the observed time dependence arises from slow binding of the inhibitors to the active site metal. However, we also found several metal binding inhibitors that exhibited rapid, non-time-dependent onset of inhibition. By a combination of structural and chemical modification studies, we show that metal binding is only slow when the rest of the inhibitor makes optimal hydrogen bonds within the subsites of PDF. Both of these interactions between the inhibitor and enzyme were found to be necessary to observe time-dependent inhibition, as elimination of either leads to its loss.

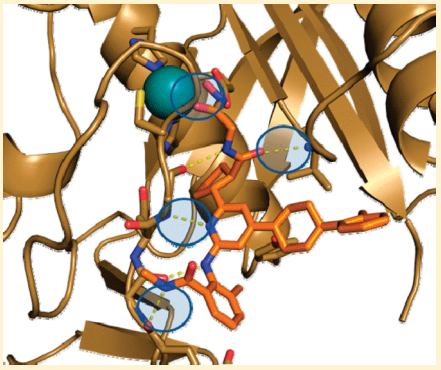

As the incidence of antimicrobial resistant infections (ARIs) continues to rise, development of new drugs has failed to keep pace.[1,2] As a result, ARIs exact a growing financial and human toll. In a recent study at one Chicago area hospital, ARIs resulted in an increased treatment cost of $30K per patient and doubled the rate of mortality.[3] Thus, the development of novel antibiotics remains an urgent, unmet medical need.

Protein synthesis in eubacteria is initiated with a formylmethionine in the first position.[4] The nascent polypeptide is then processed during translation by the enzyme polypeptide deformylase (PDF) (EC 3.5.1.88), which hydrolyzes the formyl group to liberate an unmodified methionine at the N-terminus:

$$\text{formyl-L-methionyl peptide} + H_2O \rightarrow \text{formate} + \text{methionyl peptide}$$

Seminal work from the 1960s and 1970s demonstrated that deformylation occurs after the first 40−50 amino acids are translated, rather than after synthesis of the full-length protein,[5,6] implying a form of cooperativity between PDF and the ribosome in bacteria. This has been confirmed recently in greater molecular detail, with the reported crystal structure of the 70S subunit of the ribosome complexed with the C-terminal portion of PDF.[7]

PDF has been found in all bacterial genomes sequenced to date and has been shown to be essential for viability.[8,9] Although a human form of PDF has more recently been found in mitochondria, it is thought to be a vestigial remnant of mitochondrial evolution and not to play a role in human biology. Consistent with this idea, bacterial PDF inhibitors have been shown to display no toxic effects on human cells.[10,11] Thus, inhibitors of bacterial PDF offer hope for a safe and effective treatment for current ARIs.

Actinonin is a natural product first described as an antibiotic in 1962[12] and more recently has been identified as an inhibitor of PDF.[13] Actinonin, as well as other pharmaceutically designed PDF inhibitors, has been shown to display potent, time-dependent inhibition.[14] To improve our understanding of both the origins of this slow-binding phenomenon and its importance for PDF drug discovery,[15] we have studied the mechanism of PDF inhibition with a series of GSK compounds (Figure 1). A combination of structural, mutational, and biochemical studies varying the pH, solvent isotope, and NaCl levels were conducted and showed that time-dependent inhibition of PDF results from a slow equilibration of the compounds with the active site metal. This work also showed that certain hydrogen bonding interactions

Received: April 28, 2011
Revised: June 28, 2011
Published: June 28, 2011

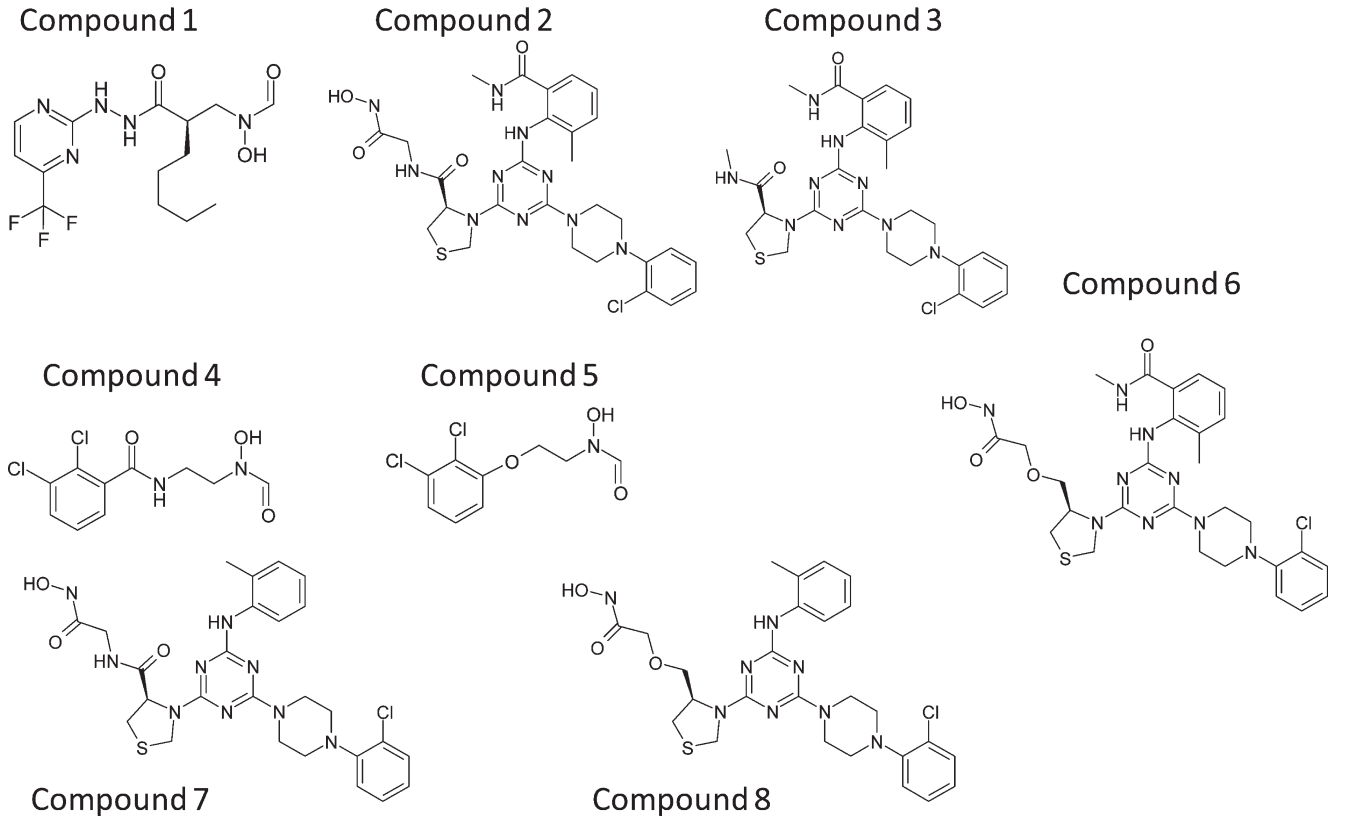

Figure 1. Structures of PDF inhibitors.

between the inhibitor and enzyme outside of metal binding were also driving the kinetics of inhibition. Implications of these results on next-generation inhibitor design are discussed.

MATERIALS AND METHODS

PDF Expression and Purification Methods. *Escherichia coli* BL21*(DE3) cells were transformed, via the heat shock method, with vectors expressing untagged forms of the wild-type (WT) and E174D PDF enzyme from *Streptococcus pneumoniae* (see the Supporting Information for details). Transformed cells were grown overnight at 37 °C in 1 L of Luria-Bertani Broth (10 g/L tryptone, 5 g/L yeast extract, and 5 g/L NaCl) with 1% glucose. Carbenicillin was added to a final concentration of 100 mg/L for selection. The 1 L overnight culture was then used to inoculate multiple 1 L shake flasks for production. Varying procedures were used on the basis of optimized conditions for soluble overexpression of WT and mutant PDF enzymes. To produce WT and the mutant E174D, MCJKLB Broth [5 g/L $(NH_4)_2SO_4$, 6 g/L K_2HPO_4, 3 g/L KH_2PO_4, 10 g/L tryptone, 5 g/L yeast extract, 5 g/L NaCl, 1% glycerol, and 0.1% glucose] was used. Growth and overnight induction with 0.05 mM IPTG occurred at 30 °C. In all cases, 0.5 mM NiCl was added 30 min prior to IPTG induction to stabilize activity. Cell paste was recovered through centrifugation using a Sorvall R12 rotor.

The following procedures were used in the purification of wild-type and mutant PDF enzymes. All the purification steps were performed at 4 °C. *E. coli* cells overexpressing PDF were homogenized and subsequently lysed by sonication in 5 volumes of lysis buffer [20 mM Tris-HCl (pH 7.5) and 5 mM nickel chloride] with protease inhibitor cocktail for use in purification of poly(histidine)-tagged proteins (Sigma). The cell lysate was collected and centrifuged at 34000*g* for 30 min. The supernatant was loaded onto a Q Sepharose Fast Flow column (50 mL bed volume, GE Healthcare). The column was washed with buffer A [20 mM Tris-HCl (pH 7.5), 5 mM nickel chloride, and 3 mM potassium phosphate] and eluted with a linear gradient from 0 to 1.0 M NaCl in buffer A. The fractions containing PDF were pooled and diluted with buffer B [20 mM Tris-HCl (pH 7) and 3 mM potassium phosphate] to reduce the concentration of NaCl. The sample was loaded onto a Mono Q HR 10/10 column (GE Healthcare), and bound proteins were eluted with a linear gradient from 0 to 0.5 M NaCl in buffer B. Fractions containing PDF were further purified with a HiLoad 16/60 Superdex 75 column (GE Healthcare) pre-equilibrated in 10 mM potassium phosphate (pH 6.8) and 150 mM NaCl. The identities of the purified proteins were confirmed by liquid chromatography–mass spectroscopy analysis and peptide mass mapping.

pH and Solvent Isotope Experiments. An acidic (25 mM potassium phosphate from monobasic, 25 mM sodium acetate, and 1 mM potassium borate, pH with phosphoric acid) and basic (25 mM potassium phosphate from tribasic, 25 mM potassium borate, and 1 mM sodium acetate, pH with KOH) combination buffer was prepared, in either protiated or deuterated solvents. The acidic and basic buffers were mixed together to obtain pH and pD values between 5 and 9, every 0.3 unit. pD values were calculated by measuring the deuterated buffers using an H_2O solution-calibrated pH electrode and adding 0.41 unit to the pH reading.[16] PDF activity was assessed using fMAS in a formate dehydrogenase (FDH)-coupled format.[17] In this assay, formate liberated from the action of PDF is oxidized to carbon dioxide concomitant with the reduction of NAD to NADH, which can

be monitored experimentally by an increase in absorbance at 340 nm. This 40 μL assay consisted of a 30 μL addition of 1.33× substrate (f-MAS, NAD, and FDH) and 10 μL of 4× enzyme in a white, clear bottom plate (Corning catalog no. 3706). The concentration of substrate was varied between 0.39 and 38 mM, and the concentration of PDF was varied between 0.5 and 2 nM for the wild-type protein, with higher concentrations being used at the extreme pH values; 50 nM *S. pneumoniae* E174D PDF was used across the entire pH or pD range. The amount of product formed was determined using a 40 min reaction. k_{cat} and K_m were determined at each pH or pD to construct the pH or pD profile.

Determination of Time-Dependent Kinetics through Progress Curve Analysis. To determine the effect of solvent and pH on the time dependence of inhibitor binding, the on rate and equilibrium constants were determined using forward progress curve analysis.[18] The concentration of inhibitor was varied from 5 nM to 100 μM in the FDH-coupled assay under various conditions, and the reactions were followed for >1 h. The k_{obs} was determined for each inhibitor concentration by fitting each progress curve to eq 2, as described in Results, and these values were then replotted and fitted to eq 3 to determine the desired kinetic values.

Determination of Compound Off Rates through Jump Dilutions. Enzyme (350 nM) and inhibitor (10 × IC_{50}) were preincubated together at room temperature for 15 min to allow for the complete onset of inhibition. This was followed by a rapid 3500-fold dilution into the FDH-coupled assay containing 40 mM ([S] > K_m) fMAS, and continuous monitoring of the recovery of enzyme activity. Controls were also run to verify that the enzyme was fully inhibited before the rapid dilution and that the enzyme was not inhibited under the final conditions. The dissociation rate constant (k_6 or more commonly the off rate) for the inhibitors was determined by fitting the progress curves to eq 3.

Viscosity Studies. The viscosity of the buffer at pH 7.7 containing between 0 and 50% sucrose was determined by measuring the migration time through an Oswalt viscometer. f-MAS was then titrated in the FDH-coupled reaction at each sucrose concentration. This 40 μL assay consisted of a 30 μL addition of 1.33× substrate (variable f-MAS, 12 mM NAD, and 60 units of FDH) and 10 μL of 4× enzyme (0.5 nM). The k_{cat} and K_m were determined at each concentration of sucrose, to determine the effect of viscosity on the reaction.

Structure Methods. At 15.5 mg/mL, *S. pneumoniae* PDF was complexed with 1 mM respective compounds for 16 h at 4 °C, and drops were applied using automated liquid handling (Mosquito, TTP Labtech) and grown over a period of 2−8 days at 22 °C in a 400 nL hanging drop. The drop was composed of 200 nL of the protein−inhibitor complex, 50 nL of previously grown crushed crystals [seeds suspended in ~3.3 M $AmSO_4$, 3% PEG 400, and 0.1 M Hepes (pH 7.5)] from apo Strep. PDF, and 150 nL of well solution [0.2 M potassium fluoride and 20% (w/v) PEG 3350]. X-ray diffraction data were collected at the Advanced Photon Source on sector 21, by the Life Sciences Collaborative Access Team. The structure was determined by molecular replacement and refined with Phenix.Refine.[19] The model was built with COOT.[20] Figures were made with Pymol.[21] X-ray data were submitted to the Protein Data Bank (PDB codes for compounds **2**, **3**, and **4** are 3STR, 3SVJ, and 3SW8, respectively).

Development of the Hydrogen Bond Strength Scoring Function. The scoring function script (scoring.svl) developed by Chemical Computing Group was used within MOE software for scoring the intermolecular interactions.[22] The scoring function coefficients were trained on a data set of ligand−receptor complexes collected from the Protein Data Bank and their published binding ΔG values.[23,24]

This scoring function generated binding energy (in kilocalories per mole) components from all of the interactions between the enzyme and inhibitor, including the intermolecular hydrogen bonds formed, the hydrophobic interactions between the protein and the ligand, the metal−ligand interactions, the flexibility of the bound ligand (bond rotation), and any water-mediated interactions. Along with these, certain physicochemical properties of the ligand alone were computed, such as cLogP, molecular weight, sum of atomic polarizabilities, and the number of hydrogen bond acceptors and donors.

The resulting model could be simplified to predict k_6 on the basis of three terms:

$$\text{predicted } pk_6 = -0.43(\text{BR}) + 0.11(\text{PLHB}) + 0.05(\text{apol}) - 0.98 \quad (1)$$

where BR is an entropic penalty term that refers to the rotatable bonds of the ligand, PLHB is the strength of the sum of the hydrogen bonds between the ligand and enzyme, and apol is the sum of the atomic polarizability of the ligand alone. The fit of predicted pk_6 versus experimental k_6 yielded an r^2 value of 0.67.

Measurement of Antimicrobial Activity. Whole-cell antimicrobial activity was determined by broth microdilution using the National Committee for Clinical Laboratory Standards (NCCLS) recommended methodology.[25] Compounds were tested in serial 2-fold dilutions ranging from 64 to 0.06 μg/mL. Strains evaluated in this assay included *S. pneumoniae* 1629, *S. pneumoniae* N1387, and *S. pneumoniae* Ery2. The minimum inhibitory concentration (MIC) was determined as the lowest concentration of compound that inhibited visible growth. A mirror reader was used to assist in determining the MIC end point.

Synthetic Methods. These are available in the Supporting Information for compounds **2**, **3**, and **6**−**8** and were previously published for compounds **1**, **4**, and **5**.[26−28]

RESULTS

Effects of pH on Catalysis and Inhibition. The pH dependence of the *S. pneumoniae* PDF-catalyzed deformylation reaction was determined by measuring reaction rates with varying substrate concentrations (0.38−39 mM) in buffers ranging in pH from 5.0 to 9.0. Data at each pH were fitted to the Michaelis−Menten equation to obtain the kinetic parameters k_{cat} and k_{cat}/K_m. These buffers contained no added chloride ion, as it has been shown to be an inhibitor of the PDF enzyme-catalyzed reaction.[29] The pH profile data were fit to an equation describing one acidic pK_a (eq 2), yielding a single of value of ~5.3 for both k_{cat} and k_{cat}/K_m (Figure 3).

$$k_{cat}(\text{obs}) = k_{cat}(\text{max})/(1 + 10^{pK_a - pH}) \quad (2)$$

The pK_a could not be determined precisely because of the instability of the protein at pH <5. However, the fitted acidic pK_a value closely matches that determined previously with the *E. coli* PDF enzyme and was shown to correspond to the active site base, Glu174, in the *S. pneumonaie* enzyme.[29,30]

A pH−rate profile was also generated for the E174D PDF protein and was similar to that of the WT enzyme (Figure 4), though the overall activity of the mutant was ~100-fold lower.

The binding kinetics and potencies of PDF inhibitors were then investigated over a range of pH values (5.5−9.2). To obtain

the parameters associated with time-dependent inhibition, progress curves were obtained at a fixed concentration of substrate (equal to its K_m value) and varying inhibitor concentrations. The resulting data were fitted to eq 3:[18]

$$P = v_s t + (v_0 - v_s)(1 - e^{-k_{obs}t})/k_{obs} \quad (3)$$

where P is the concentration of product, t is time, v_0 is the initial velocity, v_s is the final velocity, and k_{obs} is the rate of formation of the final enzyme−inhibitor complex.

The inactivation rates (k_{obs}) obtained for each inhibitor concentration were then replotted with eq 4:

$$k_{obs} = k_6 + k_5[(I/K_{i,initial})/(1 + A/K_a + I/K_{i,initial})] \quad (4)$$

where A is the concentration of the substrate, K_a is the Michaelis constant for substrate A, I is the concentration of the inhibitor, K_i is the dissociation constant for the initial step in inhibitor binding (E + I ↔ EI), and k_5 and k_6 represent the forward and reverse rate constants, respectively, for equilibration from the initial to final inhibited complex (EI ↔ EI*).

In most instances, the dissociation constant (or off rate), k_6, was too small to be determined by this method. Instead, this value was determined by classical jump dilution methods, where inhibitor is preincubated at 10 × IC_{50} concentrations with enzyme, followed by a rapid dilution below the inhibitory concentration, as reported previously with PDF and actinonin.[14] The reaction is then monitored continuously for the return of enzyme activity. The k_6 values listed in Table 1 and used in Figure 10 were determined by this method.

For apparent time-dependent inhibitors, kinetics were unchanged at acidic or neutral pH, but under basic conditions, significant changes were observed. In the fit of the data to eq 3, the rate constant k_5 was much smaller in magnitude at pH 9.2 than at pH 7.7 as demonstrated for two of the inhibitors (Figure 5). The other time-dependent parameters (K_i and k_6) were largely unchanged at pH 9.2, resulting in an overall lower potency of inhibitors at high pH, according to eq 5, where K_i^* is the overall potency of the inhibitor after full enzyme−inhibitor equilibrium has been reached:

$$K_i^* = K_i^* k_6/(k_5 + k_6) \quad (5)$$

Figure 2. Effects of inhibitor binding on protein structure. The crystal structure of apo PDF (green) was overlaid with the protein portion of a structure determined with time-dependent compound **4** (aqua). No changes in conformation were observed.

Solvent Kinetic Isotope Effects on Catalysis and Inhibition. The solvent kinetic isotope effects (sKIEs) were obtained by analysis of k_{cat} and k_{cat}/K_m versus pH or pD using the calculated maximal activity values from the fitted curves to minimize the associated errors (Figure 3). This analysis yielded the following initial sKIEs: $^D(k_{cat}/K_m) = 1.3 \pm 0.2$, and $^D(k_{cat}) = 2.0 \pm 0.2$. However, to correct for the effects of higher solvent viscosity in deuterated buffers, the effects of viscosity on k_{cat} and k_{cat}/K_m were determined by measuring PDF activity in buffers with varying sucrose concentrations. There was no viscosity effect observed on k_{cat}/K_m but a measurable effect on k_{cat} (k_{cat0}/k_{cat} vs $\eta/\eta_0 = 0.4$). The relative viscosity of the deuterated buffers used in this study was determined to be ~1.1, and the appropriate correction was made to the observed sKIEs, yielding a corrected $^D(k_{cat}/K_m)$ of 1.2 and a corrected $^D(k_{cat})$ of 1.9. sKIE values were also obtained for the E174D PDF, with the following corrected values determined: $^D(k_{cat}/K_m) = 1.3 \pm 0.1$, and $^D(k_{cat}) = 1.2 \pm 0.1$ (Figure 4).

The binding of inhibitors was next studied as a function of solvent. Using eqs 3 and 4, progress curves for PDF inhibitors were studied in protiated (pH 7.7) and deuterated buffers (pD 7.7). Because of the relatively invariant pH profile, determinations were made at only single pH or pD values. The rate constant k_5 was determined to be faster in deuterated buffer for time-dependent inhibitors. Taking the ratio of k_5 values in the different buffers resulted in an inverse sKIE value on $^Dk_5$ of 0.6 ± 0.1 for compound **2** (Figure 6A) and 0.4 ± 0.1 for compound **1** (Figure 6B).

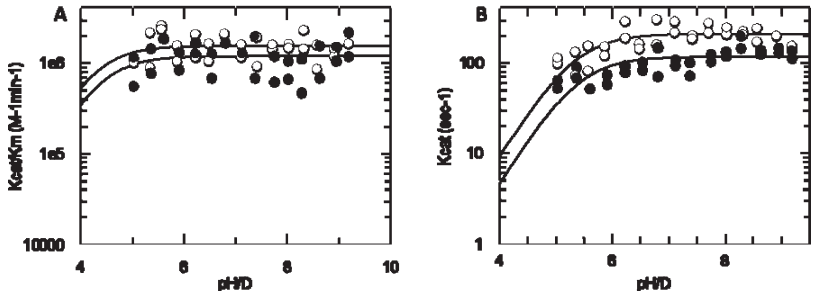

Figure 3. pH/pD profiles for wild-type *S. pneumoniae* PDF. PDF activity was measured in the FDH-coupled assay in buffers with varying pH (○) and pD (●) values. Profiles for k_{cat}/K_m (A) and k_{cat} (B) were fitted to eq 2, a model with one acidic pK_a value.

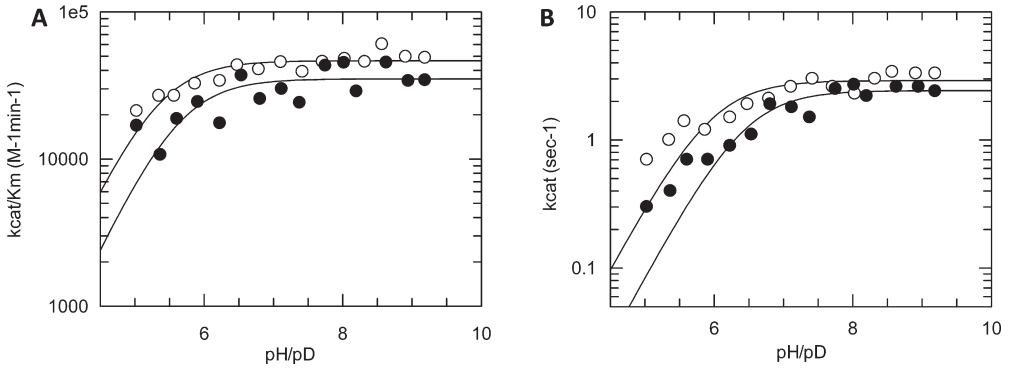

Figure 4. pH/pD profile of E174D *S. pneumoniae* PDF. Mutant PDF activity was measured as with the WT enzyme, and k_{cat}/K_m (A) and k_{cat} (B) values are displayed as a function of pH (○) or pD (●).

Table 1. Binding Kinetics of PDF Inhibitors

	K_i (nM)	k_5 (s^{-1})	k_6 (s^{-1})	K_i^{*a} (nM)
compound **1**	6309	0.0225	0.000253	70.24
compound **2**	334	0.0171	0.000205	3.96
compound **3**	117	n/a[b]	n/a[b]	n/a[b]
compound **4**	25910	0.0177	0.000212	306.18
compound **5**	31720	n/a[b]	n/a[b]	n/a[b]
compound **6**	213	0.0292	0.000158	1.15
compound **7**	650	0.0408	0.000518	8.15
compound **8**	53.7	n/a[b]	n/a[b]	n/a[b]

[a] K_i^* values were calculated from K_i, k_5, and k_6 using eq 5. [b] Not applicable because compounds are not time-dependent.

Effects of Chloride on Catalysis and Inhibition. Chloride has previously been shown to inhibit the *E. coli* PDF by virtue of competing with water for binding to the active site metal.[29] Chloride was shown to inhibit our *S. pneumoniae* PDF similarly (Figure 7A) with an IC_{50} of ~70 mM. It should be noted that in control experiments, ionic strength itself had no effect on enzyme activity up to 300 mM (data not shown).

The binding kinetics of our inhibitors were then studied under standard conditions (pH 7.7, no chloride added) and under conditions of high salt (pH 7.7, 300 mM chloride). After the progress curves had been fit as described above, the main effect of chloride is to decrease the value of the time-dependent binding microscopic rate constant k_5 by nearly 10-fold (Figure 7B).

Determination of Structures of Compounds 2 and 3. Data from crystals of PDF cocrystallized with compounds **2** and **3** were collected to 1.75 and 1.5 Å resolution, respectively (Table 2). Both crystals contain one molecule per asymmetric unit, and both respective compounds are clearly visible in the active site (Figure 8). Compounds **2** and **3** bind identically to the protein except for compound **2** binding to the active site metal. Other important interactions, such as direct hydrogen bonds to V71, E126, and G127, are conserved between the two.

DISCUSSION

The most potent PDF inhibitors have been developed both from natural product sources and by design.[31−33] Though these compounds were shown to be time-dependent, a detailed understanding of why they display this characteristic is not known. Thus, we began a detailed analysis of our time-dependent inhibitors with *S. pneumoniae* PDF.

The substrate binding site of *S. pneumoniae* PDF revels a central α helix (α-7) flanked by β sheets above and below this helix. At the far end of the pocket is a set of conserved residues, HEXXH, that coordinate the catalytic metal along with a conserved cysteine (C130) residue. With other enzyme targets, time dependence is often associated with domain movements that accompany inhibitor binding.[34−36] However, a comparison of the crystal structures for *S. pneumoniae* PDF reveals that the shape, size, and electrostatics of the different pockets and the location of the residues remain unaltered between the apo structure and the structure for *S. pneumoniae* PDF with a time-dependent inhibitor (Figure 2). Thus, the time dependence of our PDF inhibitors is not due to induced fit types of changes. It should be noted that this is in contrast to a recent publication with the *Arabidopsis thaliana* deformylase.[37] However, as noted in that paper, there are unique conformational states observed crystallographically with the plant enzyme that have not been reported with PDFs from other sources. Indeed, in our own work, we have obtained numerous structures (both apo and with ligand bound) of PDF from *S. pneumoniae* and have observed only a single form of the enzyme.

We next considered whether the slow binding of our compounds was related to their interaction with the active site metal. Time-dependent inhibition has been investigated with zinc proteases such as stromelysin and thermolysin and in those cases was ascribed to displacement of the metal-bound water by the inhibitor.[38,39] Though PDF contains iron as the biologically relevant cofactor,[40] it is related to the zinc protease family, containing several conserved family motifs, most notably the canonical HEXXH helix that contains the active site glutamate base.[41] To test whether the slow binding behavior of our PDF inhibitors is the result of binding to the metal in PDF, we varied pH and solvent and observed the effects of these parameters on the time-dependent kinetics. These values are expected to change in predicted ways depending on the mechanism of the slow binding step in PDF inhibitor binding.

It should be noted that these studies were performed on the nickel-containing *S. pneumoniae* form of PDF. Though iron is the relevant biological metal, it is highly unstable and difficult with which to work, because of oxidation of the metal.[42] However, it has been shown that either nickel or cobalt can substitute for iron and yield very similar catalytic activities and inhibition profiles. Nickel and cobalt forms of PDF are also more stable and therefore

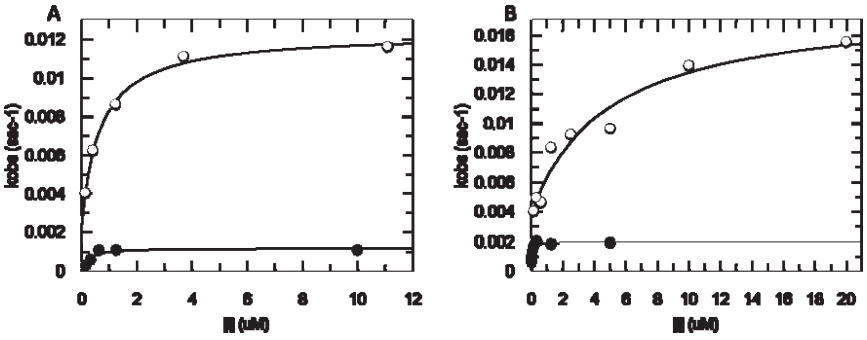

Figure 5. Determination of time-dependent kinetics at neutral and high pH. Progress curves were determined at varying concentrations of compound **2** (A) and compound **1** (B) at pH 7.7 (○) and 9.2 (●). Progress curves were initially fit to eq 3 to determine k_{obs} values, which were then replotted with eq 4 to yield the hyperbolic fits shown here.

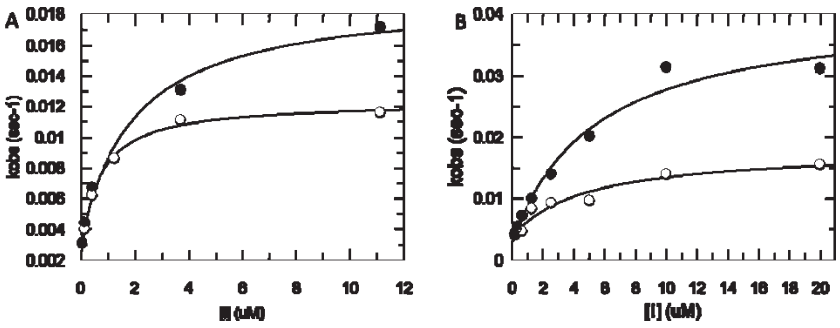

Figure 6. Determination of solvent kinetic isotope effects (sKIEs) on time-dependent kinetics. Progress curves were determined at varying concentrations of compound **2** (A) and compound **1** (B) in buffer of pH 7.7 (○) and pD 7.7 (●). Progress curves were initially fit to eq 3 to determine k_{obs} values, which were then replotted with eq 4 to yield the hyperbolic fits shown here.

make kinetic studies possible under aerobic conditions.[29,43] This is in contrast to the zinc form of the enzyme, which displays activity 2−3 orders of magnitude lower than that of the iron form. This has been ascribed to the stronger ability of iron, nickel, and cobalt as compared to zinc to adopt the presumed five-coordinate geometry necessary for catalysis,[44,45] though there have been a few notable exceptions in which zinc appears to be the relevant in vivo metal.[46,47]

pH and solvent were initially examined for their effects on catalysis. A thorough understanding of the catalytic mechanism is needed as a backdrop for examinations of inhibition. A relatively pH invariant profile was observed with *S. pneumoniae* PDF for both k_{cat} and k_{cat}/K_m (Figure 3), consistent with previous profiles determined for the *E. coli* form of the enzyme.[29] A single, acidic pK_a was fitted to the data, yielding a value of ∼5.3. However, this value potentially corresponding to the active site glutamate (E174)[29,30] cannot be fitted precisely because of the instability of the protein at pH <5.

Solvent kinetic isotope effects (sKIEs) were next examined by generating comparable rate data in deuterated buffers across a similar pH or pD range (Figure 3). There was a small, normal sKIE on k_{cat}/K_m [$^D(k_{cat}/K_m)$ = 1.3 ± 0.2] and a much larger normal sKIE on k_{cat} [$^D(k_{cat})$ = 1.9 ± 0.2]. The differences in these values of $^D(k_{cat}/K_m)$ and $^D(k_{cat})$ may reflect the fact that the second half-reaction of PDF, which is expressed in $^D(k_{cat})$, but not $^D(k_{cat}/K_m)$, is overall rate-limiting for the wild-type enzyme. Both values were corrected for the viscosity effects inherent to deuterated buffers, and the measured viscosity effect on enzyme activity ($k_{cat}/K_{m0}/k_{cat}/K_m$ vs $\eta/\eta_0 = 0$; k_{cat0}/k_{cat} vs $\eta/\eta_0 = 0.4$).

We derived expressions for $^D(k_{cat}/K_m)$ and $^D(k_{cat})$ (eqs 6 and 7, respectively) based on the mechanism outlined in Scheme 1 (with solvent sensitive steps highlighted in red).

$$^D(k_{cat}/K_m) = [^Dk_3 + k_3/k_2 + (k_4/k_5)^DK_{eq3}{}^Dk_5]/(1 + k_3/k_2 + k_4/k_5) \quad (6)$$

$$^D(k_{cat}) = \{^Dk_9 + {}^DK_{eq9}(k_{10}/k_{11}) + k_9/k_{11} + k_9/k_7 + {}^Dk_5(k_9/k_5) + k_9/k_3[^Dk_3 + {}^Dk_5{}^DK_{eq3}(k_4/k_5)]\}/[1 + k_{10}/k_{11} + k_9/k_{11} + k_9/k_7 + k_9/k_5 + k_9/k_3(1 + k_4/k_5)] \quad (7)$$

One can calculate the equilibrium solvent isotope effects $^DK_{eq\ 3}$ and $^DK_{eq\ 9}$ through the reversible solvent sensitive steps k_3 and k_9, based on the fractionation factors (ϕ) for the various reactant and product species. For $^DK_{eq\ 3}$, a large inverse equilibrium effect is expected, driven by the low value of 0.69 for the ϕ of M−OL$^+$ bonds[48] found in the reactants for step k_3, and thus in the numerator of the equilibrium expression (eq 8):

$$^DK_{eq3} = \phi(\text{M−OL})^2\phi(\text{CONL})/\phi(\text{CO}_2\text{L})\phi(\text{M−OL})\phi(\text{CONL})^{tetra} = 0.56 \quad (8)$$

For $^DK_{eq\ 9}$, a large normal equilibrium effect is calculated, driven by the same low value of 0.69 for the ϕ of M−OL$^+$ bonds, which are now found on the product side of this step, as

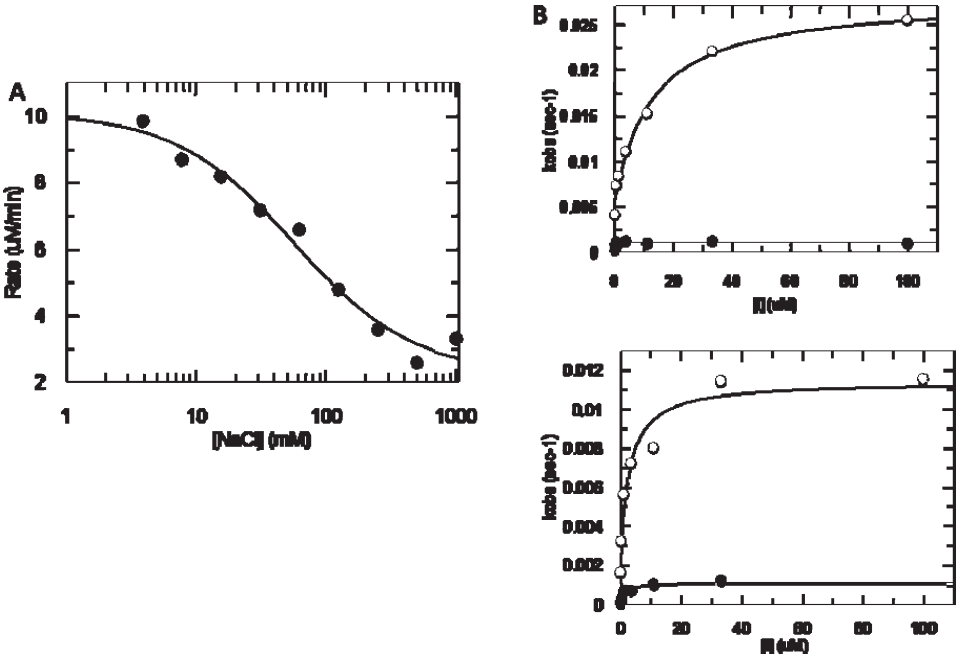

Figure 7. Effects of NaCl on time-dependent kinetics. (A) An IC_{50} for NaCl was determined in the standard FDH-coupled PDF assay at pH 7.7. Fitting data to a standard four-parameter fit yielded an IC_{50} of 70 mM. (B) Progress curves were determined at varying concentrations of compound **2** (top) and compound **1** (bottom) in a buffer free of chloride (○) and with 300 mM Cl (●). PDF activity was monitored at pH 7.7 by following NAD reduction at 340 nm in the FDH-coupled assay.[16] Progress curves were initially fit to eq 3 to determine k_{obs} values, which were then replotted with eq 4 to yield the hyperbolic fits shown here.

water displaces formate from the metal in step k_9 to regenerate the active form of the enzyme:

$$^{D}K_{eq\ 9} = \phi(CO_2L)\phi(OL)^2/\phi(CO_2L)\phi(M{-}OL^+)^2 = 2.1 \quad (9)$$

To help simplify solutions for eqs 6 and 7, we studied a mutant of the putative active site base, glutamate 174. E174D had an ~100-fold reduction in both k_{cat} and k_{cat}/K_m values. As E174 is involved in deprotonation of the metal-bound water (step k_3 in Scheme 1), the decrease in activity observed with this mutant is likely due to this step becoming rate-limiting in E174D. Consistent with this idea, the large sKIE of 1.9 ± 0.2 observed in k_{cat} for the wild-type enzyme has decreased to 1.2 ± 0.1 in the mutant, virtually identical to the value for k_{cat}/K_m (Figure 4), and the viscosity effect observed on wild-type k_{cat} has been abolished.

The fact that the E174D mutant of PDF is thought to exhibit a diminished value of k_3 and the fact that values of $^{D}(k_{cat})$ and $^{D}(k_{cat}/K_m)$ are experimentally identical are consistent with the proposal that the sKIEs of the mutant enzyme arise solely from the first half-reaction (steps $k_1{-}k_5$). Re-examination of eqs 6 and 7 for the E174D mutant enzyme demonstrates that expressions for $^{D}(k_{cat}/K_m)$ and $^{D}(k_{cat})$ would be identical under conditions where $k_3 \ll k_2$ and $k_9/k_3 \gg 1$: $^{D}(k_{cat}/K_m) = [^{D}k_3 + (k_4/k_5)^{D}K_{eq\ 3}\ ^{D}k_5]/(1 + k_4/k_5) \sim {}^{D}(k_{cat}) = (k_9/k_3)[^{D}k_3 + {}^{D}k_5\ ^{D}K_{eq\ 3}(k_4/k_5)]/[(k_9/k_3)(1 + k_4/k_5)]$. If $k_4/k_5 = 0$ for the E174D enzyme, both $^{D}(k_{cat})$ and $^{D}(k_{cat}/K_m)$ express the intrinsic solvent isotope effect on k_3 ($^{D}k_3 = 1.2{-}1.3$), while if $k_4/k_5 \gg 1$, $^{D}(k_{cat}) = {}^{D}(k_{cat}/K_m) = {}^{D}k_5\ ^{D}K_{eq\ 3} = 1.2{-}1.3$, where $^{D}k_5 = 2.1{-}2.3$. Accordingly, for the wild-type enzyme, the experimental value of $^{D}(k_{cat})$ (1.9 ± 0.2) could reflect the case in which the second half-reaction is more rate-limiting than the first half-reaction (k_3, $k_5 \ll k_9$) such that the expression for $^{D}(k_{cat})$ simplifies to eq 10 for which $^{D}k_9 > 1$ and $^{D}K_{eq\ 9} = 2.1$:

$$^{D}(k_{cat}) = [^{D}k_9 + {}^{D}K_{eq9}(k_{10}/k_{11})]/(1 + k_{10}/k_{11}) \quad (10)$$

This is reasonable given that given that the k_3 step involves prototropic steps, the k_5 step involves the breakdown of the high-energy tetrahedral intermediate, while the k_9 step involves both protonation and the breakdown of a bidentate chelate.

Having a more complete understanding of PDF kinetics, we then studied the effects of pH and sKIE on PDF inhibition. The time-dependent inhibition of compounds **1** and **2** was studied at low, neutral, and basic pH values. There was little change between neutral (7.7) and acidic pH (5.5), but we did observe a large change in going to basic pH (9.2) values (Figure 5). In fitting the data to eq 3, we obtained a 10−11-fold decrease in the k_5 value at high pH values. In considering relevant functional groups, the pK_a of nickel-bound water is found to range from 8.2 for model systems to 8.7 for urease.[49,50] If a slow step in binding of the compounds to the enzyme involves displacement of the metal-bound water, k_5 would be expected to be much slower at high pH when the water is deprotonated to form a metal-bound hydroxide. The relative binding affinities for water and hydroxide have been studied in the cobalt form of *E. coli* PDF, where it was found that hydroxide binds much more tightly.[29] Thus, the effects of pH on time-dependent inhibition are consistent with the hypothesis that the slow step is due to binding of the compounds to the active site metal with concomitant displacement of water.

To further probe this possibility, the kinetics of inhibitor binding were compared in protiated and deuterated buffers.

Table 2. Crystallographic Data[a]

	2	3
	Data Collection	
space group	$P4_3$	$P4_3$
cell dimensions		
a, *b*, *c* (Å)	50.2, 50.3, 91.5	50.4, 50.4, 92.5
α, β, γ (deg)	90, 90, 90	90, 90, 90
resolution (Å)	50−1.75 (1.81−1.75)	50−1.55 (1.61−1.55)
R_{sym} or R_{merge}	0.076 (0.442)	0.045 (0.420)
$I/\sigma I$	19.7 (2.8)	35.2 (2.4)
completeness (%)	99.9 (99.6)	99.9 (99.8)
redundancy	5 (4.8)	4.8 (4.3)
beamline	APS 21IDf	ALS-502
	Refinement	
resolution (Å)	28−1.75	33−1.55
no. of reflections	21704	31783
R_{work}/R_{free}	0.19/0.23	0.16/0.20
no. of atoms		
protein	1520	1520
ligand	44	40
water/ion	90	107
B factor (Å^2)		
protein	27.4	26.1
ligand	28.9	34.5
water/ion	35.1	30.7
root-mean-square deviation		
bond lengths (Å)	0.006	0.005
bond angles (deg)	1.045	0.996

[a] Values in parentheses are for the highest-resolution shell.

Consistently, we observed a significant, inverse solvent isotope effect on k_5 across our inhibitors. $^{D}k_5$ was equal to 0.6 ± 0.1 for compound **2** (Figure 6A) and 0.4 ± 0.1 for compound **1** (Figure 6B). The finding of an inverse solvent isotope effect is unique and diagnostic of the involvement of a few specific functional groups. As discussed with the sKIEs on k_{cat}, M−OL$^+$ bonds have an associated ϕ value of 0.69, which using the rule of geometric mean would contribute a value of 0.69^2 = 0.48 to the overall equilibrium effect. The fact that the observed kinetic effect is close to the equilibrium value indicates that the transition state is very productlike in character (i.e., full displacement of the water from the metal) and importantly provides strong evidence that the slow step in our inhibitor binding comes from binding to the active site metal.

Finally, this hypothesis was tested by measuring inhibitor kinetics in the presence of a ligand that competes for binding to the active site metal of PDF. If a ligand with greater affinity is included, k_5 should decrease for reasons similar to high pH; i.e., displacement of a ligand stronger than water will affect the inhibitor kinetics if metal binding is the slow step in compound binding. Chloride was chosen for these studies, as it has been shown to be a good inhibitor of *E. coli* PDF, and its inhibition mechanism (binding to the metal) has been assigned unambiguously by spectroscopic methods.[29] We determined the potency of chloride with the *S. pneumoniae* nickel-containing PDF to be ∼70 mM (Figure 7A), similar to the value determined for the *E. coli* cobalt-containing PDF.[29] Next, we determined the binding kinetics for compounds **1** and **2** either in the absence of chloride or with the competing ligand present at 300 mM. We observed a significant decrease in k_5 (Figure 7B) for both compounds in the presence of chloride. It should be noted that we chose compounds with similar metal chelating functionalities but with diverse central scaffolds to emphasize that the results described above are not a function of the chemical class of the compound studied.

All of the kinetic data support the hypothesis that the time dependence of PDF inhibitors is due to slow binding to the active site metal of the enzyme. To chemically test this hypothesis, we compared the structures and kinetics (Figure 8A) of two compounds that are identical except for the presence of a metal chelating group. Compound **2**, which contains the metal binding scaffold, was found to be time-dependent, whereas compound **3**, which lacks the ability to bind the metal, did not display any time dependence, as judged by its progress curves. An overlay of the crystal structures of these two inhibitors (Figure 8B) shows clearly that there are no changes in the protein conformation or protein−inhibitor interactions between these two compounds, except the binding to the active site metal by compound **2**.

In terms of efficacy, the slow binding compound **2** displays MIC values of 4−16 μg/mL across the three strains of *S. pneumoniae* tested (1629, N1387, and Ery2), whereas the non-time-dependent compound **3** displays no apparent antimicrobial effects (MICs of >64 μg/mL against all three strains). Though these compounds are good exemplars for comparison on the basis of their close structural analogy, the argument could be made that their overall potencies (Table 1) could account for the differences in their MIC values. Alternatively, compound **1** (70 nM) and compound **3** (114 nM) display similar overall potencies, even though only compound **1** binds to the active site metal and displays time-dependent inhibition. While there was an absence of antimicrobial activity with compound **3**, compound **1** exhibited MIC values of 4−16 μg/mL. Thus, time-dependent inhibition is a hallmark of compounds with cellular efficacy.

Though the evidence described above shows that the time-dependent binding of our GSK compounds is due to slow binding to the active site metal, an interesting question is whether metal binding is itself sufficient for slow binding kinetics. Another way to ask this question is whether all metal binding compounds are time-dependent inhibitors of PDF.

In fact, we have several compounds that bind to the active site metal in crystal structures but are not time-dependent, implying that other molecular interactions modulate the kinetics of this system. To improve our understanding of these secondary contributions, we studied the interactions between the PDF inhibitors and key residues on the protein. These residues were chosen on the basis of designed interactions as well as spontaneous resistance mutation experiments. The latter is in analogy to previous work, where we showed that resistance mutations in HIV integrase caused our inhibitors to lose their time-dependent properties.[51] In the case of PDF, both the spontaneous mutations and the knowledge-based efforts identified many of the same inhibitor−protein interactions (Figure 9A). For example, Val71 (*S. pneumoniae* PDF) sits in the substrate binding site and through design donates a hydrogen bond from the backbone amide NH group to an acceptor in the inhibitor (compound **4**).

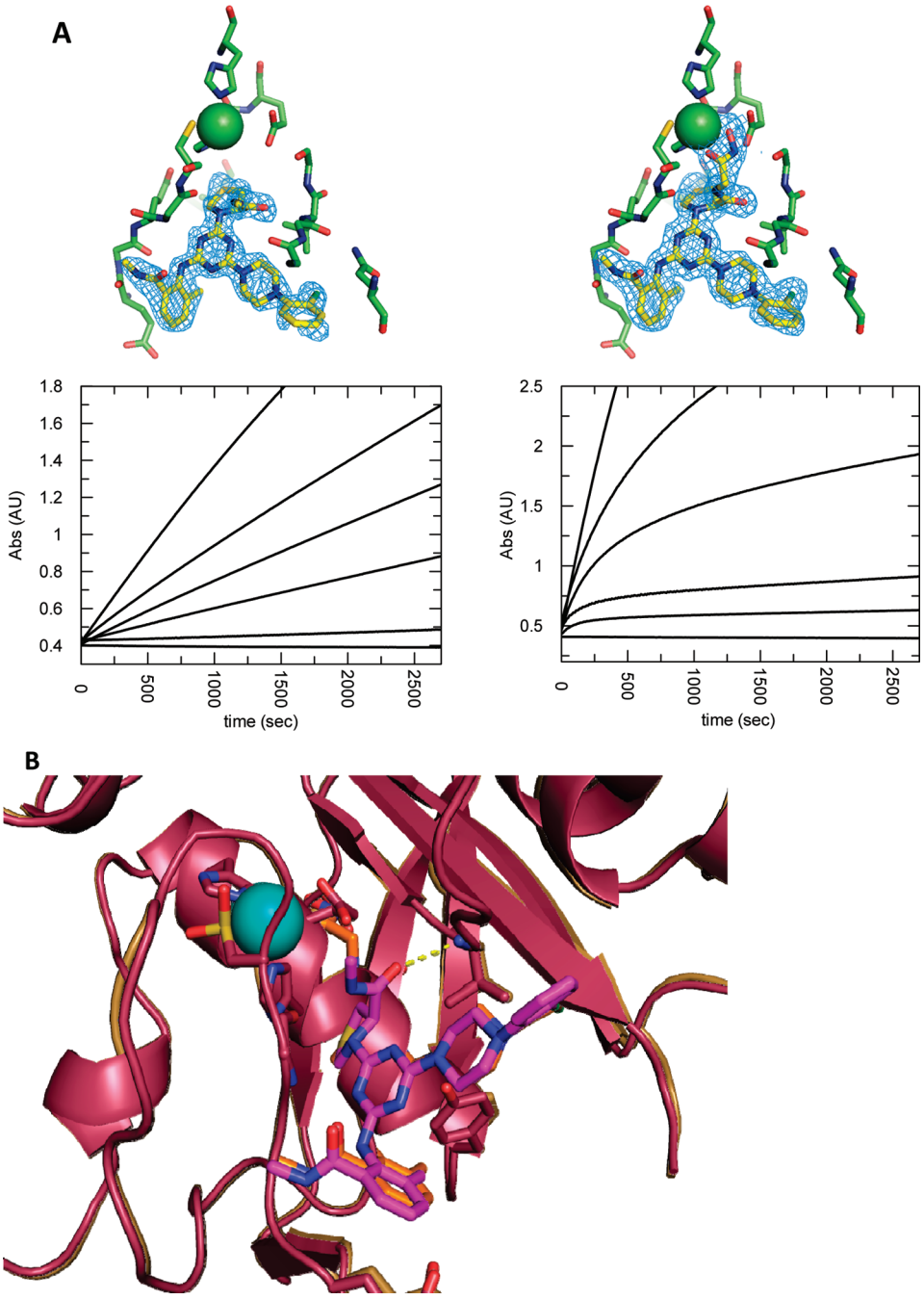

Figure 8. (A) Electron density and progress curves for compound **3** (left) and compound **2** (right). Compound **3** was judged to be non-time-dependent on the basis of the linear progress curves, whereas compound **2** was judged to be time-dependent on the basis of the nonlinear curves. PDF activity was monitored at pH 7.7 as described in the legend of Figure 7. Respective electron densities are contoured at 1σ. (B) Overlay of PDF structures with compound **2** (orange) and compound **3** (purple). No conformational changes or differences in hydrogen bonding to the protein were observed between the two structures, except for the ability of compound **2** to bind to the active site metal (green sphere).

To test whether this interaction contributes to the time-dependent inhibitor binding, we made an analogue, compound **5**, in which the hydrogen bond acceptor for Val71 has been removed by replacement of an amide by an ether functionality. This compound binds to the active site metal in a fashion equivalent to that of compound **4** but is no longer time-dependent, as judged by the linear progress curves (Figure 9B). It is important to note that compounds **4** and **5** display very different overall potencies (Table 1), despite that fact that both contain the same metal chelating group. Thus, it appears that interactions both with the metal and with the surrounding protein matrix are critical determinants of inhibitor SAR and time dependence.

This result provides a single example in which changes in hydrogen bonding between PDF and the inhibitor help modulate the rate of binding to the active site metal. To see if this hypothesis is true more broadly, we developed a QSAR model for time dependence based on the measured off rates of a larger set of compounds. The model was developed from both the

Scheme 1. Proposed Catalytic Mechanism for Ni-Containing PDF[a]

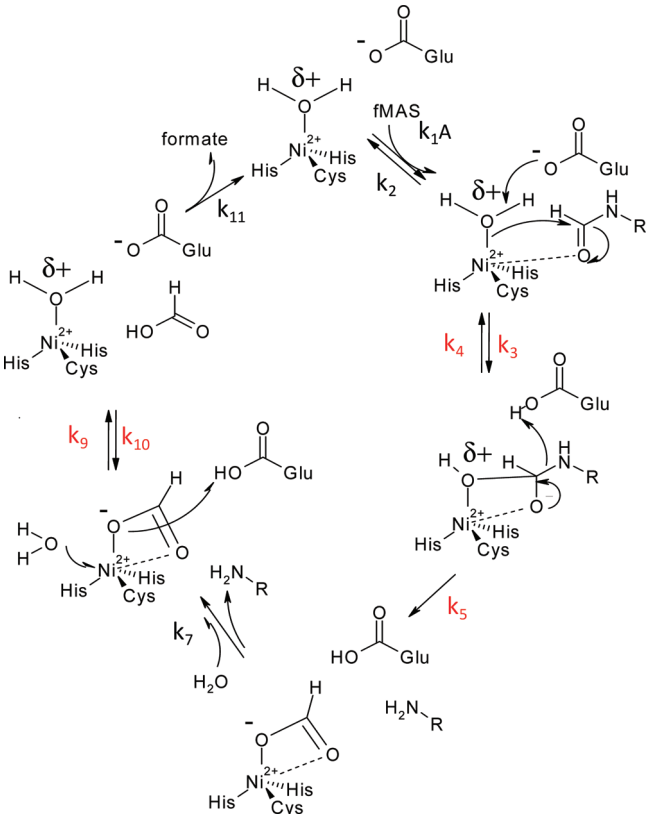

[a] Steps sensitive to the solvent isotope are highlighted in red.

interactions between the inhibitors and PDF and the physiochemical properties of the ligands alone. On the basis of relevance, only three terms are predicted to affect the k_6, or off rate, of the compounds (eq 1):

$$\text{predicted } pk_6 = -0.43(\text{BR}) + 0.11(\text{PLHB}) + 0.05(\text{apol}) - 0.98 \quad (1)$$

The PLHB term describes the sum of the hydrogen bonds between the inhibitor and the enzyme. The coefficient is positive for this term, indicating that the compounds are predicted to display more time dependence as the number of hydrogen bonds is increased. The apol term, which also correlates positively with the predicted pk_6 value, describes the polarizability of the ligand, which captures its ability to bind to the active site metal and surrounding water molecules. Thus, in general our model predicts that binding to both the active site metal and the surrounding protein residues is predicted to increase the time dependence of our PDF inhibitors. The bond rotation term (BR) describes the entropic cost of constraining rotatable bonds upon binding to the enzyme. The coefficient is negative for this parameter, suggesting that more flexible molecules are less time-dependent. This may arise from poorer hydrogen bonds being formed between PDF and flexible portions of the inhibitor due to configurational entropy. As a validation of this model, a plot of the predicted and experimental off rates displayed a good ($r^2 = 0.67$) correlation (Figure 10).

A prediction from this finding is that scaffolds with more hydrogen bonds should be better able to retain their time dependence when losing key interactions with the protein, which might occur in the clinic from resistance mutations. For example, in a comparison of compounds **2** and **4**, both make identical hydrogen bonds to Val71 and Gly129, but compound **2** in addition has key interactions with Gly72, Glu126, and Gly127. To test this hypothesis, we explored a series of compounds with the same core structure as compound **2**. Within the context of this scaffold, we observe that after removal of the hydrogen bond to the backbone of Val71 by changing on the inhibitor an amide to an ether group (compound **2** vs compound **6**) we still maintain time-dependent inhibition. In fact, the kinetics and overall potency of the compound are largely unchanged (Table 1). Note that this was the same chemical change made to the chemical scaffold of compound **4**, where time-dependent binding was lost.

Other protein−inhibitor interactions can be removed from compound **2** with similar results. For example, we abolished the hydrogen bond between compound **2** and the backbone NH group of E126 by chemical means (compound **7**), and again the compound retains potent, time-dependent inhibition (Table 1). In fact, for this scaffold, we need to remove several key hydrogen bonding interactions in tandem (compound **8**) to lose the time-dependent binding.

It should be noted that we chose to change the compound functionalities rather than make mutants of PDF to test the importance of individual hydrogen bonding interactions. This decision was based on the fact that PDF contributes mainly backbone functionalities, and it was not straightforward to make side chain mutations and reliably predict how this would be transmitted to the key inhibitor−protein hydrogen bonding interactions. We felt it was much easier to simply remove the portion of the inhibitor involved in the interaction of interest.

In summary, we have shown that the weight of kinetic evidence supports the hypothesis that the time-dependent nature of PDF inhibition arises from binding of the compounds to the active site metal of PDF. This is in analogy to previous work done with metal binding inhibitors of zinc proteases, and underlies the fact that PDF shares much of the same functionality and mechanism of zinc proteases, even though biology has chosen a different metal as the cofactor for PDF.

In addition, we have shown that metal binding by these inhibitors is not an intrinsically slow process but rather requires some context by the rest of the inhibitor. An important influence in this regard is the hydrogen bonding network between the inhibitor and certain key residues of the protein, including Val71. The exact reason for why these interactions help to modulate the rate of binding to the active site metal is not known at present. In all of the inhibitor-bound crystal structures of *S. pneumoniae* PDF obtained at GSK, the metal chelating groups adopt the same geometry on the metal. Thus, one possibility is that there is a greater entropic barrier for binding to the metal if the rest of the inhibitor is conformationally constrained within the active site of PDF. To test this possibility, we are producing isotopically labeled PDF for NMR studies.

An implication from this work is that the time dependence of our PDF inhibitors can be retained in the face of losses of key hydrogen bonds by judicious choice of the chemical scaffold. In the clinic, this could result in drugs that are more able to withstand resistance mutations and allow for a longer effective lifetime in the healthcare community. We plan to test this

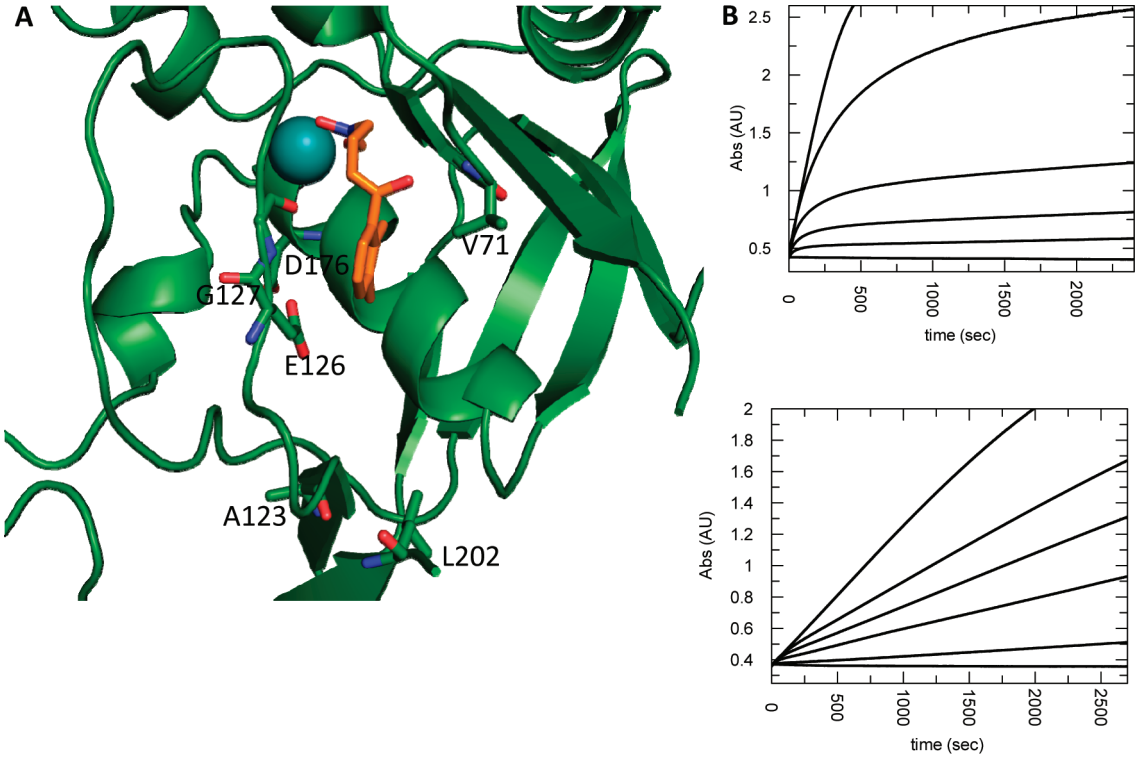

Figure 9. (A) Map of spontaneous resistance mutations in *S. pneumoniae* PDF. Crystal structure of compound **4** annotated with the residues found to lead to spontaneous resistance. (B) Progress curves were determined for compound **4** (top) and compound **5** (bottom). PDF activity was monitored at pH 7.7 as described in the legend of Figure 7. Compound **5** was judged to be non-time-dependent on the basis of the linear progress curves, whereas compound **4** was judged to be time-dependent on the basis of the nonlinear curves.

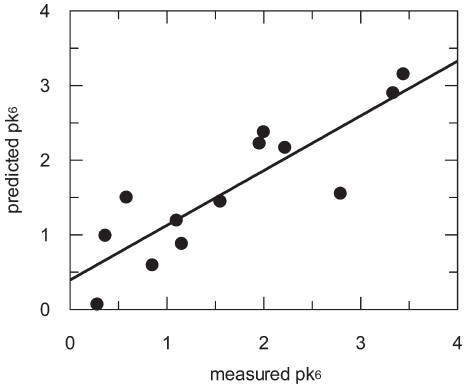

Figure 10. Correlation between predicted and experimental off rates. The off rates (or k_6 values) were determined by rapid dilution methods for 13 compounds that were predicted from a QSAR model to display a range of time-dependent inhibition. The correlation between the predicted and experimental pk_6 values is plotted, along with a linear fit to the data.

hypothesis by comparing the hydrogen bond forming abilities of compounds with the rate of resistance mutations in in vitro experiments.

■ ASSOCIATED CONTENT

Supporting Information. Derivation of eqs 6 [$^{D}(k_{cat}/K_m)$] and 7 [$^{D}(k_{cat})$], analytical characterization of wild-type and E174D PDF from *S. pneumonia*, and synthetic methods for compounds **2**, **3**, and **6**−**8**. This material is available free of charge via the Internet at http://pubs.acs.org.

■ AUTHOR INFORMATION

Corresponding Author

*Phone: (610) 917-6740. Fax: (610) 917-7385. E-mail: Benjamin.2.Schwartz@gsk.com.

■ ABBREVIATIONS

PDF, polypeptide deformylase; ARIs, antimicrobial resistant infections; FDH, formate dehydrogenase; sKIE, solvent kinetic isotope effect.

■ REFERENCES

(1) Projan, S. J., and Shlaes, D. M. (2004) Antibacterial drug discovery: Is it all downhill from here? *Clin. Microbiol. Infect. 10*, 18–22.

(2) Infectious Diseases Society of America (2004) Bad Bugs, No Drugs: As antibiotic discovery stagnates a public health crisis brews. http://www.idsociety.org/badbugsnodrugs.html.

(3) Roberts, R. R., Hota, B., Ahmad, I., Scott, R. D., Foster, S. D., Abbasi, F., Schabowski, S., Kampe, L. M., Ciavarella, G. G., Supino, M., Naples, J., Cordell, R., Levy, S. B., and Weinstein, R. A. (2009) Hospital and societal costs of antimicrobial-resistance infections in a Chicago teaching hospital: Implications for antibiotic stewardship. *Clin. Infect. Dis. 49*, 1175–1184.

(4) Marcker, K., and Sanger, F. (1964) N-Formyl-methionyl-S-RNA. *J. Mol. Biol. 8*, 835–840.

(5) Adams, J. M. (1968) On the release of the formyl group from nascent protein. *J. Mol. Biol. 33*, 571–589.

(6) Ball, L. A., and Kaesberg, P. (1973) Cleavage of the N-terminal formylmethioine residue from a bacteriophage coat protein *in vitro*. *J. Mol. Biol. 79*, 531–537.

(7) Bingel-Erlenmeyer, R., Kohler, R., Kramer, G., Sandikci, A., Antolic, S., Maier, T., Schaffitzel, C., Wiedmann, B., Bukau, B., and Ban, N. (2007) A peptide deformylase-ribosome complex reveals mechanism of nascent chain processing. *Nature 452*, 108–111.

(8) Meinnel, T., and Blanquet, S. (1994) Characterization of the *Thermus thermophilus* locus encoding peptide deformylase and methionyl-tRNA$_f$ formyltransferase. *J. Bacteriol. 176*, 7387–7390.

(9) Mazel, D., Pochet, S., and Marliere, P. (1994) Genetic characterization of polypeptide deformylase, a distinctive enzyme of eubacterial translation. *EMBO J. 13*, 914–923.

(10) Nguyen, K. T., Hu, X., Colton, C., Chakrabarti, R., Zhu, M. X., and Pei, D. (2003) Characterization of a human peptide deformylase: Implications for antibacterial drug design. *Biochemistry 42*, 9952–9958.

(11) Serero, A., Giglione, C., Sardini, A., Martinez-Sanz, J., and Meinnel, T. (2003) An unusual peptide deformylase features in the human mitochondrial N-terminal methionine excision pathway. *J. Biol. Chem. 278*, 52953–52963.

(12) Gordon, J. J., Kelly, B. K., and Miller, G. A. (1962) Actinonin: An antibiotic substance produced by an actinomycete. *Nature 195*, 701–702.

(13) Chen, D. Z., Patel, D. V., Hackbarth, C. J., Wang, W., Dreyer, G., Young, D. C., Margolis, P. S., Wu, C., Ni, Z.-J., Trias, J., White, R. J., and Yuan, Z. (2000) Actinonin, a naturally occurring antibacterial agent, is a potent deformylase inhibitor. *Biochemistry 39*, 1256–1262.

(14) Val Aller, G. S., Nandigama, R., Petit, C. M., DeWolf, W. E., Quinn, C. J., Aubart, K. M., Zalacain, M., Christensen, S. B., Copeland, R. A., and Lai, Z. (2005) Mechanism of time-dependent inhibition of polypeptide deformylase by actinonin. *Biochemistry 44*, 253–260.

(15) Copeland, R. A., Pompliano, D. L., and Meek, T. D. (2006) Drug-target residence time and its implication for lead optimization. *Nat. Rev. Drug Discovery 5*, 730–739.

(16) Glasoe, P. K., and Long, F. A. (1960) Use of glass electrodes to measure acidities in deuterium oxide. *J. Phys. Chem. 64*, 188–189.

(17) Lazennec, C., and Meinnel, T. (1997) Formate dehydrogenase coupled spectrophotometric assay of peptide deformylase. *Anal. Biochem. 244*, 180–182.

(18) Morrison, J. F., and Walsh, C. T. (1988) The behavior and significance of slow-binding enzyme inhibitors. *Adv. Enzymol. 61*, 201–301.

(19) Adams, P. D., Grosse-Kunstleve, R. W., Hung, L.-W., Ioerger, T. R., McCoy, A. J., Moriarty, N. W., Read, R. J., Sacchettini, J. C., Sauter, N. K., and Terwilliger, T. C. (2002) PHENIX: Building new software for automated crystallographic structure determination. *Acta Crystallogr. D58*, 1948–1954.

(20) Emsley, P., and Cowtan, K. (2004) Coot: Model-building tools for molecular graphics. *Acta Crystallogr. D60*, 2126–2132.

(21) DeLano, W. L. (2009) *The PyMOL Molecular Graphics System*, DeLano Scientific LLC, Palo Alto, CA.

(22) Bondarev, D. scoring.svl, available from SVL exchange (svl.chemcomp.com) (December 28, 2005) Molecular Operating Environment (MOE), 2010.10; Chemical Computing Group Inc., Montreal.

(23) Eldridge, M. D., Murray, C. W., Auton, T. R., Paolini, G. V., and Mee, R. P. (1997) Empirical scoring functions: I. The development of a fast empirical scoring function to estimate the binding affinity of ligands in receptor complexes. *J. Comput.-Aided Mol. Des. 11*, 425–445.

(24) Baxter, C. A., Murray, C. W., Clark, D. E., Westhead, D. R., and Eldridge, M. D. (1998) Flexible Docking Using Tabu Search and an Empirical Estimate of Binding Affinity. *Proteins 33*, 367–382.

(25) NCCLS Document M7-A5 (2000) Methods for Dilution Antimicrobial Susceptibility Tests for Bacteria that Grow Aerobically, 5th ed.

(26) Aubart, K. M., Benowitz, A. B., Christensen, S. B., IV, Karpinski, J. M., Lee, J., and Silva, D. J. (2003) PCT Int. Appl. WO 2003101442 A1.

(27) Karpinski, J. M., Christensen, S. B., Aubart, K. M., Van Aller, G. S., DeMarsh, P. L., Lewandowski, T. F., Rittenhouse, S., Kulkarni, S. G., McIntyre, T. A., Woods, L. C., et al. (2005) *Abstracts of Papers*, 229th ACS National Meeting, San Diego, March 13−17, 2005, American Chemical Society, Washington, DC.

(28) Aubart, K. M., Christensen, S. B., IV, and Briand, J. (2001) PCT Int. Appl. WO 2001085170 A1.

(29) Rajagopalan, P. T. R., Grimme, S., and Pei, D. (2000) Characterization of cobalt(II)-substituted peptide deformylase: Function of the metal ion and the catalytic residue Glu-133. *Biochemistry 39*, 779–790.

(30) Deng, H., Callender, R., Zhu, J., Nguyen, K. T., and Pei, D. (2002) Determination of the ionization state and catalytic function of Glu-133 in peptide deformylase by difference FTIR spectroscopy. *Biochemistry 41*, 10563–10569.

(31) Aubart, K., and Zalacain, M. (2006) Peptide deformylase inhibitors. *Prog. Med. Chem. 44*, 109–143.

(32) Hu, X., Nguyen, K. T., Verlinde, C. L. M. J., Hol, W. G. J., and Pei, D. (2003) Structure-based design of a macrocyclic inhibitor for peptide deformylase. *J. Med. Chem. 46*, 3771–3774.

(33) Sharma, A., Khuller, G. K., and Sharma, S. (2009) Peptide deformylase: A promising therapeutic target for tuberculosis and antibacterial drug discovery. *Expert Opin. Ther. Targets 13*, 753–765.

(34) Sullivan, T. J., Truglio, J. J., Boyne, M. E., Novichenok, P., Zhang, X., Stratton, C. F., Li, H. J., Kaur, T., Amin, A., Johnson, F., Slayden, R. A., Kisker, C., and Tonge, P. I. (2006) High affinity InhA inhibitors with activity against drug-resistant strains of *Mycobacterium tuberculosis*. *ACS Chem. Biol. 1*, 43–53.

(35) Wood, E. R., Truesdale, A. T., McDonald, O. B., Yuan, D., Hassell, A., Dickerson, S. H., Ellis, B., Pennisi, C., Horne, E., Lackey, K., Alligood, K. J., Rusnak, D. W., Gilmer, T. M., and Shewchuk, L. (2004) A unique structure for epidermial growth factor bound to GW572016 (Lapatininb): Relationships among protein conformation, inhibitor off-rate, and receptor activity in tumor cells. *Cancer Res. 64*, 6652–6659.

(36) Pagellis, C., Tong, L., Churchill, L., Cirillo, P. F., Gilmore, T., Graham, A. G., Grob, P. M., Hickey, E. R., Moss, N., Pav, S., and Regan, J. (2002) Inhibition of p38 MAP kinase by utilizing a novel allosteric binding site. *Nat. Struct. Biol. 9*, 268–272.

(37) Fieulaine, S., Boularot, A., Artaud, I., Desmadril, M., Dardel, F., Meinnel, T., and Giglione, C. (2011) Trapping conformational states along ligand-binding dynamics of peptide deformylase: the impact of induced fit on enzyme catalysis. *PLoS Biol. 9*, No. e1001066.

(38) Izquierdo-Martin, M., and Stein, R. L. (1992) Mechanistic studies on the inhibition of thermolysin by a peptide hydroxamic acid. *J. Am. Chem. Soc. 114*, 325–331.

(39) Izquierdo-Martin, M., Chapman, K. T., Hagmann, W. K., and Stein, R. L. (1994) Studies on the kinetic and chemical mechanism of stromelysin by an N-(carboxyalkyl)dipeptide. *Biochemistry 33*, 1356–1365.

(40) Rajagopalan, P. T. R., Yu, C., and Pei, D. (1997) Peptide deformylase: A new type of mononuclear iron protein. *J. Am. Chem. Soc. 119*, 12418–12419.

(41) Dardel, F., Ragusa, S., Lazennec, C., Blanquet, S., and Meinnel, T. (1998) Solution structure of nickel-peptide deformylase. *J. Mol. Biol. 280*, 501–513.

(42) Rajagopalan, P. T. R., and Pei, D. (1998) Oxygen-mediated inactivation of peptide deformylase. *J. Biol. Chem. 273*, 22305–22310.

(43) Ragusa, S., Blanquet, S., and Meinnel, T. (1998) Control of peptide deformylase activity by metal cations. *J. Mol. Biol. 280*, 515–523.

(44) Jain, R., Hao, B., Liu, R., and Chan, M. K. (2005) Strucutres of *E. coli* peptide deformylase bound to formate: Insight into the preference for Fe^{2+} over Zn^{2+} as the active site metal. *J. Am. Chem. Soc. 127*, 4558–4559.

(45) Wu, X., Quan, J., and Wu, Y. (2007) Theoretical study of the catalytic mechanism and metal-ion dependence of peptide deformylase. *J. Phys. Chem. 111*, 6236–6244.

(46) Huang, J., Van Aller, G. S., Taylor, A. N., Kerrigan, J. J., Liu, W.-S., Trulli, J. M., Lai, Z., Holmes, D., Aubart, K. M., Brown, J. R., and Zalacain, M. (2006) Phylogenomic and biochemical characterization of three *Legionella pneumophila* polypeptide deformylases. *J. Bacteriol. 188*, 5249–5257.

(47) Nguyen, K. T., Wu, J.-C., Boylan, J. A., Gherardini, F. C., and Pei, D. (2007) Zinc is the metal cofactor of *Borrelia burgdorferi* peptide deformylase. *Arch. Biochem. Biophys. 468*, 217–225.

(48) Schowen, K. B. J. (1978) Solvent hydrogen isotope effects. In *Transition States of Biochemical Processes* (Gandour, R. D., and Schowen, R. L., Eds.) pp 225−283, Plenum Press, New York.

(49) Guo, Y., Ge, Q., Lin, H., and Zhu, S. (2003) Synthesis, thermodynamic properties and kinetics of the acid-catalyzed dissociation of nickel(II) diamido polyamino complexes. *Transition Met. Chem. (Dordrecht, Neth.) 28*, 668–675.

(50) Yamaguchi, K., Cosper, N. J., Stalhandske, C., Scott, R. A., Pearson, M. A., Karplus, P. A., and Hausinger, R. P. (1999) Characterization of metal-substituted *Klebsiella aerogenes* urease. *J. Biol. Inorg. Chem. 4*, 468–477.

(51) Garvey, E. P., Schwartz, B., Gartland, M. J., Lang, S., Halsey, W., Sathe, G., Carter, H. L., and Weaver, K. L. (2009) Potent inhibitors of HIV-1 integrase display a two-step, slow binding inhibition mechanism which is absent in a drug-resistant T66I/M154I mutant. *Biochemistry 48*, 1644–1653.